

Annamalai Selvam^{1*}, Santiago John Mary¹, Asirvatham Ajila¹, Devadoss Delinta¹, Vijayagopal Sribharathy², Senthamarai Kannan Muthukumaran³

¹Department of Chemistry, Loyola Institute of Frontier Energy (LIFE), Loyola College, Chennai-600 034, Tamil Nadu, India, ²Department of Chemistry, Anna Adhars College for Women, Chennai-600 040, Tamil Nadu, India, ³Department of Chemistry, Ramakrishna Mission Vivekananda College, Chennai-600 004, Tamil Nadu, India

Scientific paper

ISSN 0351-9465, E-ISSN 2466-2585

<https://doi.org/10.62638/ZasMat1004>



Zastita Materijala 65 (1)
110 - 125 (2024)

Electrochemical activities of Ni-Ti alloy in artificial blood plasma with *Trigonella foenum graecum* seeds

ABSTRACT

An investigation of the electrochemical behaviour of Ni-Ti alloy when exposed to artificial blood plasma (ABP) in the presence of 0.1 and 0.5 ppm of *Trigonella foenum graecum* (TFG) seeds for 1, 10, 20, and 30 days. Studies on AC impedance and polarisation have shown that a protective coating forms on the metal surface while inhibiting corrosion. The protective film has formed on the Ni-Ti implant alloy surface, the linear polarization resistance increased (LPR), and the corrosion current value (I_{corr}) decreased. The charge transfer resistant value (R_{ct}) and impedance value increase and the double-layer capacitance value decrease. The protective layers morphology and the elemental composition were analyzed by SEM/EDAX. The property of the protective film on the Ni-Ti alloy has been examined by atomic force microscope. The X-ray diffraction analysis has confirmed the nature of the apatite. The corrosion inhibition efficiency of Ni-Ti alloy in ABP in the presence of TFG seeds at various concentrations for different times was improved and protected.

Keywords: Nickel-titanium, AFM, protective film, Nyquist plots, Bode plots

1. INTRODUCTION

Nickel-Titanium alloy, known as nitinol, has been used in orthopedic and orthodontic applications because of its attractiveness and exceptional properties. It possesses super elasticity and shape memory effect. Due to its excellent biocompatibility, which is comparable with that of Ti, along with shape memory and super elasticity properties, Ni-Ti alloy draws more attention in biomedical applications than other metallic constituents [1]. The Ni-Ti SMAs are among the most popular SMAs for biomedical applications, including stents or medical and dental wires, due to the relative ease of formability and improved fracture and fatigue resistance compared with other commercial shape memory alloys [2]. The Ni-Ti alloys in the medical field provide significant advantages and new treatment options in various medical cases.

*Corresponding author: Annamalai Selvam

E-mail: selvamchemist@gmail.com

Paper received: 25. 09. 2023.

Paper accepted: 25. 10. 2023.

Paper is available on the website: www.idk.org.rs/journal

However, metallic ion release, particularly Ni release, still requires a more profound understanding for improved safety and biocompatibility of this class of alloys in the human body, especially for long-term treatments. The Ni release occurs as a result of the interaction of the alloy with tissue or body fluids. It depends on the alloy type, tissue or body fluid surrounding it, and the type and morphology of the possible oxide layers forming on the alloy. Each parameter affects how the alloy's chemical, mechanical, and surface properties change within the body, affecting the materials biocompatibility. Among these parameters, passive oxide layer formation is more critical in affecting the Ni release. Compared to Ni, Ti is chemically a more reactive metal and can easily segregate at the surface and form an oxide layer when exposed to atmospheric or aqueous conditions. Ti can form various oxides, including TiO, Ti₂O₃, and TiO₂ [3,4]. The various metals and alloys have been used as biomaterials whose corrosion resistance has been investigated in artificial body fluids, various metals, and alloys such as Co-Cr-Mo alloys [5, 6], Cr-Ni stainless steel, Cr-Ni-Mo stainless steel [7]. According to reports, fenugreek has hypocholesterolemic, anti-diabetic, anti-cancer,

anti-microbial, and anti-parasitic properties [8]. The production of therapeutic medicines is due to the many compounds in fenugreek seeds and leaves.

In general, fenugreek contains three important constituents with medicinal value: (i) 4-hydroxy isoleucine, (ii) galactomannans, and (iii) steroidal saponins. These constituents have placed fenugreek among the most commonly recognized 'nutraceutical' or health food products [9]. The TFG seeds are helpful in heart disease and aphrodisiac and as a galactagogue promoting lactation [10]. Being a natural health product, it can treat and cure diseases, thus providing medical and health benefits. It has therefore been regarded as a possible nutraceutical [11]. This study was designed to investigate the effect of Ni-Ti alloy in artificial blood plasma in the presence of TFG seeds. This study reveals that the intake of TFG seeds containing Fenugreekine increases immunity. The various concentrations of seeds were prepared, and their inhibition efficiency of TFG in the artificial blood plasma for 1, 10, 20, and 30 days has been examined by Potentiodynamic polarization, AC impedance spectroscopy, SEM analysis, EDAX, AFM, and XRD techniques.

By directly giving some naturally occurring phytoproducts to diabetic patients to assist in controlling their blood sugar levels, it is possible to measure the corrosion activity of metal alloys under various environments. *Trigonella foenum graecum* seeds were employed in this investigation as an anti-diabetic.

2. MATERIALS AND METHODS

2.1. Materials

The metal specimen, Ni-Ti alloy composition Ti = 50.1, Ni = 40.2, and C = 9.7 wt. %. The chemical composition of artificial blood plasma was prepared in the laboratory, according to PN-EN ISO 10993-15 standard (g/l distilled water) was NaCl=6.8, CaCl₂=0.2, KCl=0.4, NaH₂PO₄=0.026, NaHCO₃=2.2, Na₂HPO₄=0.126, MgSO₄=0.1 [12]. The pH of artificial blood plasma was 7.4, used as an electrolyte in the electrochemical studies.

The *Trigonella foenum graecum* seeds were bought in the local market. The seed powder was weighed and dissolved in ethanol. Two different extracts were obtained, namely aqueous and ethanol extracts [13]. The different concentrations of these extracts were used for the experiment to characterize the nutrients which contain the hetero atoms, and π electrons act as suitable inhibitors.

2.2. Methods

A CHI660A workstation model was used in the electrochemical studies. The Tafel plot was obtained from potentiodynamic polarization studies

as a potential versus log (i) plot. The corrosion potential (E_{corr}) and corrosion current (I_{corr}) were deduced from the Tafel plot.

The corrosion current is obtained using the Stern-Geary equation 1 [14].

$$I_{corr} = \frac{\beta_a \times \beta_c}{2.3 R_p (\beta_a \times \beta_c)} \dots\dots\dots(1)$$

where

β_a and β_c are the Tafel slopes of the anodic and cathodic part of Tafel plot and R_p is polarization resistance.

A polarization study was utilised to calculate the linear polarisation resistance (LPR), corrosion potential (E_{corr}), and corrosion current (I_{corr}) of ABP in the presence and absence of TFG seeds.

AC impedance spectra were recorded in the same instrument used for the polarization study, using the same type of three-electrode cell assembly. The charge transfer resistance (R_{ct}) values and double-layer capacitance (C_{dl}) were calculated. From the results, analyze the protective film formation on the Ni-Ti alloy surface and know the systematic aspects of corrosion resistance. AC impedance was achieved using the CHI660A. The impedance were recorded with initial E (v) = 0; low frequency (Hz) = 10; high frequency (Hz) = 1×10^5 ; amplitude (V) = 0.005 and quit time (s) = 2 [15].

2.3. Characterizations

Subsequently, the surface morphology of the protective film after exposure to ABP in the presence of TFG seeds of 0.5 ppm was characterized using SEM spectroscopy. EDAX spectra were used to accomplish the elemental composition of the Ni-Ti alloy surface in the presence and absence of TFG seeds.

However, more definite characterizations of Ni-Ti alloy surface morphology in the presence of TFG seeds in ABP solution will be performed with the use of some new atomic force microscopy and X-ray diffraction investigations.

3. RESULTS AND DISCUSSION

3.1. *Trigonella foenum graecum* seeds

TFG seeds were ground into powder and then defatted by petroleum ether. The different alkaloids, saponin, and flavonoids are to be found in TFG, but saponin is to be found to be a high-level concentration in the TFG [16]. Plant tissue cultures from seeds grown under optimal conditions have produced as much as 2% diosgenin with fewer quantities of gitongenin and trigogenin. The significant components of TFG seeds are high carbohydrates, proteins, flavonoids, alkaloids, saponin, free amino acids, glycosides,

mucilage, minerals, and much more [17]. Further investigations have shown its effectiveness in diminishing blood glucose levels, treating gastric abnormalities, on lowering cholesterol [18].

3.2. Potentiodynamic polarization study

A polarization study has been used to confirm the formation of a protective film on the alloy surface during the corrosion inhibition process. The

protective film is formed on the Ni-Ti alloy surface, the linear polarization resistance increases (LPR), and the corrosion current value (I_{corr}) decreases. Figure 1 to 4 shows the polarization curves of Ni-Ti alloy exposed in ABP in the absence and presence of TFG seeds at various concentrations for various time intervals. (Table 1) embraces the corrosion parameters, specifically I_{corr} , E_{corr} , and LPR.

Table 1. Results of potentiodynamic polarization measurements for Ni-Ti alloy

Tabela 1. Rezultati merenja potenciodinamičke polarizacije za Ni-Ti leguru

Days	Alloy	System	E_{corr} mV vs. SCE	β_c mV/decade	β_a mV/decade	LPR ($\Omega \cdot \text{cm}^2$)	I_{corr} (A/cm^2)
1 Day	Ni-Ti	ABP	-513	137	376	1.8789×10^6	2.331×10^{-8}
		ABP /TFG 0.1ppm	-693	131	386	1.9769×10^6	2.230×10^{-8}
		ABP /TFG 0.5ppm	-618	137	376	2.0478×10^6	2.085×10^{-8}
10 Days		ABP	-626	150	406	9.0947×10^5	5.250×10^{-8}
		ABP /TFG 0.1ppm	-579	150	270	1.3144×10^6	3.391×10^{-8}
		ABP /TFG 0.5ppm	-692	160	283	2.5225×10^6	1.668×10^{-8}
20 Days		ABP	-494	141	504	5.3967×10^5	8.900×10^{-8}
		ABP /TFG 0.1ppm	-570	148	304	1.4747×10^6	2.917×10^{-8}
		ABP /TFG 0.5ppm	-585	151	284	2.0936×10^6	2.073×10^{-8}
30 Days	ABP	-509	149	443	5.0664×10^5	9.620×10^{-8}	
	ABP /TFG 0.1ppm	-615	166	286	1.7446×10^6	2.621×10^{-8}	
	ABP /TFG 0.5ppm	-786	122	306	2.0997×10^6	1.816×10^{-8}	

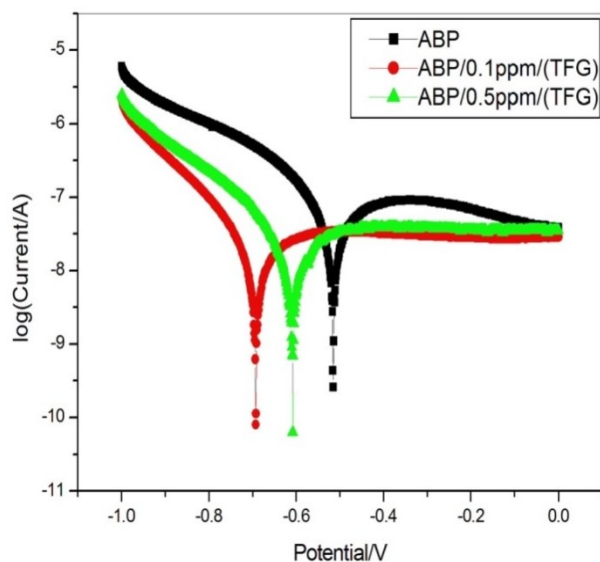


Figure 1. Polarization curves of Ni-Ti alloy exposed in ABP in the absence and presence of TFG seeds for 1 Day

Slika 1. Polarizacione krive legure Ni-Ti izložene u ABP u odsustvu i prisustvu semena TFG tokom 1 dana

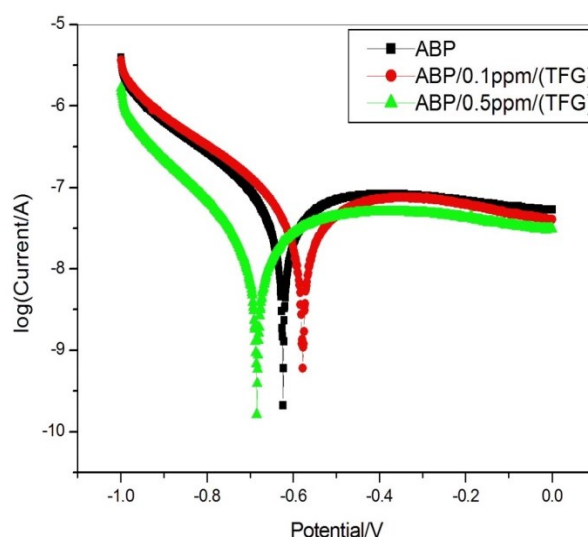


Figure 2. Polarization curves of Ni-Ti alloy exposed in ABP in the absence and presence of TFG seeds for 10 Days

Slika 2. Krive polarizacije legure Ni-Ti izložene u ABP u odsustvu i prisustvu TFG semena tokom 10 dana

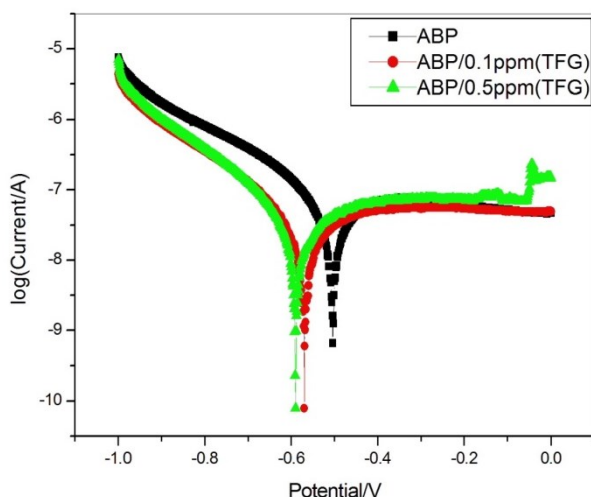


Figure 3. Polarization curves of Ni-Ti alloy exposed in ABP in the absence and presence of TFG seeds for 20 Days

Slika 3. Polarizacione krive legure Ni-Ti izložene u ABP u odsustvu i prisustvu TFG semena tokom 20 dana

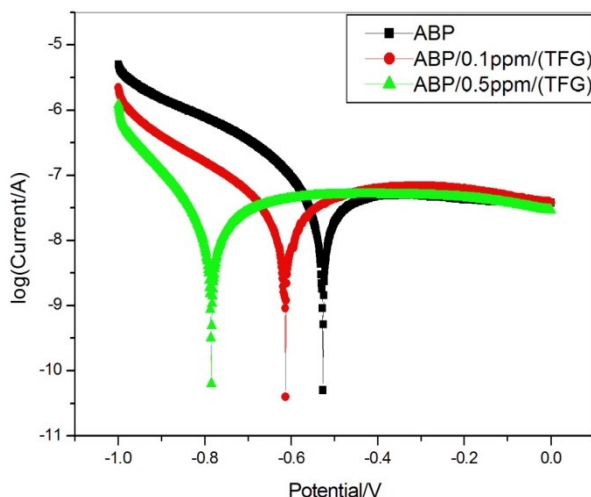


Figure 4. Polarization curves of Ni-Ti alloy exposed in ABP in the absence and presence of TFG seeds for 30 Days

Slika 4. Krive polarizacije legure Ni-Ti izložene u ABP u odsustvu i prisustvu TFG semena tokom 30 dana

The Ni-Ti alloy is immersed in ABP in the absence of TFG seeds for 1 day, the corrosion potential is -513 mV vs SCE, as shown in (Table 1). The LPR value is 1.8789×10^6 ohm.cm², and the corrosion current (I_{corr}) is 2.331×10^{-8} A/cm². The Tafel slopes ($b_c = 137$ mV/decade, $b_a = 376$ mV/decade). Similarly, when the Ni-Ti alloy is immersed in ABP in the presence of 0.1 ppm and 0.5 ppm of TFG seeds for 1 day, the potential

corrosion shifts from -513 mV vs. SCE to -693 mV vs. SCE and -618 mV vs. SCE, as shown in (Table 1). The LPR value increases from 1.8789×10^6 ohm.cm² to 1.9769×10^6 ohm.cm² and 2.0478×10^6 ohm.cm². The corrosion current (I_{corr}) value decreases from 2.331×10^{-8} A/cm² to 2.230×10^{-8} A/cm² and 2.085×10^{-8} A/cm². The Tafel slopes from ($b_c = 137$ mV/decade, $b_a = 376$ mV/decade) to ($b_c = 131$ mV/decade, $b_a = 386$ mV/decade) and ($b_c = 137$ mV/decade, $b_a = 376$ mV/decade) indicate that the rate of change of corrosion current with potential is much higher during anodic polarisation than during cathodic polarisation.

The Ni-Ti alloy is immersed in ABP in the absence of TFG seeds for 10 days, the corrosion potential is -626 mV vs. SCE, as shown in (Table 1). The LPR value is 9.094×10^5 ohm.cm² and the corrosion current (I_{corr}) is 5.250×10^{-8} A/cm². The Tafel slopes ($b_c = 150$ mV/decade, $b_a = 406$ mV/decade). Similarly, when the Ni-Ti alloy is immersed in ABP in the presence of 0.1 ppm and 0.5 ppm of TFG seeds for 10 days, the potential corrosion shifts from -626 mV vs. SCE to -579 mV vs. SCE and -692 mV vs. SCE, as shown in (Table 1). The LPR value increases from 9.0947×10^5 ohm.cm² to 1.3144×10^6 ohm.cm² and 2.5225×10^6 ohm.cm². The corrosion current (I_{corr}) decreases from 5.250×10^{-8} A/cm² to 3.391×10^{-8} A/cm² and 1.668×10^{-8} A/cm². The Tafel slopes from ($b_c = 150$ mV/decade, $b_a = 406$ mV/decade) to ($b_c = 150$ mV/decade, $b_a = 270$ mV/decade) and ($b_c = 160$ mV/decade, $b_a = 283$ mV/decade) indicate that the rate of change of corrosion current with potential is much higher during anodic polarisation than during cathodic polarisation. An oxide film is formed on the Ni-Ti alloy surface during anodic polarisation.

The Ni-Ti alloy is immersed in ABP in the absence of TFG seeds for 20 days, the corrosion potential is -494 mV vs. SCE, as shown in (Table 1). The LPR value is 5.3967×10^5 ohm.cm², and the corrosion current (I_{corr}) is 8.900×10^{-8} A/cm². The Tafel slopes ($b_c = 141$ mV/decade, $b_a = 504$ mV/decade). Similarly, when the Ni-Ti alloy is immersed in ABP in the presence of 0.1 ppm and 0.5 ppm of TFG seeds for 20 days, the potential corrosion shifts from -494 mV vs. SCE to -570 mV vs. SCE and -585 mV vs. SCE, as shown in (Table 1). The LPR value increases from 5.3967×10^5 ohm.cm² to 1.4743×10^6 ohm.cm² and 2.0936×10^6 ohm.cm². The corrosion current (I_{corr}) decreases from 8.900×10^{-8} A/cm² to 2.917×10^{-8} A/cm² and 2.073×10^{-8} A/cm². The Tafel slopes from

(bc =141 mV/decade, ba =504 mV/decade) to (bc =148 mV/decade, ba =304 mV/decade) and (bc =151 mV/decade, ba =284 mV/decade) indicate that the rate of change of corrosion current with potential is much higher during anodic polarisation than during cathodic polarisation. An oxide film is formed on the Ni-Ti alloy surface during anodic polarisation.

The Ni-Ti alloy is immersed in ABP in the absence of TFG seeds for 30 days, the corrosion potential is -509 mV vs. SCE, as shown in (Table 1). The LPR value is 5.0664×10^5 ohm.cm², and the corrosion current (I_{corr}) is 9.620×10^{-8} A/cm². The Tafel slopes (bc =149 mV/decade, ba = 443 mV/decade). Similarly, when the Ni-Ti alloy is immersed in ABP in the presence of 0.1 ppm and 0.5 ppm of TFG seeds for 30 days, the potential corrosion shifts from -509 mV vs. SCE to -615 mV vs. SCE and -786 mV vs. SCE, as shown in (Table 1). The LPR value increases from 5.0664×10^5 ohm.cm² to 1.7446×10^6 ohm.cm² and 2.0997×10^6 ohm.cm². The corrosion current (I_{corr}) decreases from 9.620×10^{-8} A/cm² to 2.621×10^{-8} A/cm² and 1.816×10^{-8} A/cm². The Tafel slopes from (bc=149 mV/decade, ba = 443 mV/decade) to (bc=166 mV/decade, ba =286 mV/decade) and (bc=122 mV/decade, ba =306 mV/decade) indicate that the rate of change of corrosion current with potential is much higher during anodic polarisation than during cathodic polarisation. An oxide film is formed on the Ni-Ti alloy surface during anodic polarisation.

The LPR rises, and the fall in corrosion current (I_{corr}) shows that the formation of a protective layer on the Ni-Ti implant alloy surface blocks the active sites and inhibits the corrosion, and weakens the rate of corrosion [19].

It is fascinating to note that the Ni-Ti in the presence of TFG seeds at 0.1 ppm and 0.5 ppm concentrations are immersed for 1, 10, 20 and 30 days, the rate of corrosion decreases, and the corrosion current also decreases, thereby showing in the LPR and I_{corr} values. This indicates that a compelling protective film is formed more on the alloy surface in the presence of TFG seeds for 30 days.

3.3. Analysis of Alternating Current impedance spectra

The equivalent circuit diagram of being immersed in ABP in the presence of 0.1 ppm and 0.5 ppm TFG seed concentrations for 1, 10, 20, and 30 days have shown in Figure 5 [20, 21]. The corrosion process is generally inhibited if the phase angle is greater than 45°.

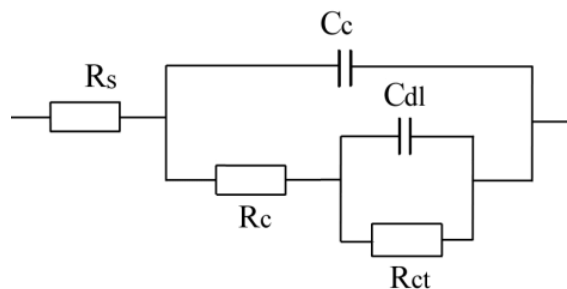


Figure 5. Equivalent circuit diagram

Slika 5. Ekvivalentna šema kola

R_{ct} = charge transfer resistance,

C_{dl} = double layer capacitance,

C_c = capacitance of the coating

The same kind of three-electrode cell assembly was utilised to record AC impedance spectra on the identical apparatus that was used for the polarisation investigation. At different frequencies, the cell impedance's real part Z' and imaginary part Z'' were measured in ohms. Double layer capacitance (C_{dl}) and charge transfer resistance (R_t) values were computed.

$$R_t = (R_s + R_t) - R_s \quad \text{.....(2)}$$

where

R_t = total resistance

R_s = solution resistance

$$C_{dl} = \frac{1}{2\pi f_{max} R_{ct}} \quad \text{.....(3)}$$

where

f_{max} = maximum frequency

The Ni-Ti alloy is immersed in ABP without TFG seeds for 1 day, the charge transfer resistance (R_{ct}) is 90 ohm.cm². The double layer capacitance (C_{dl}) is 1.766×10^{-8} F/cm², shown in (Table 2). The impedance value is 3.80 log (Z/ohm), as shown in (Figure 6(b)). The Bode phase graph shows the phase angle at 84°. Hence, the corrosion process is inhibited. When Ni-Ti alloy is immersed in ABP containing 0.1 ppm and 0.5 ppm of TFG seeds for 1 day, the R_{ct} value increases from 90 ohm.cm² to 180 ohm.cm² and 200 ohm.cm². The C_{dl} value decreases from 1.766×10^{-8} F/cm² to 8.83×10^{-9} F/cm² and 7.8×10^{-9} F/cm² shown in (Table 2). (Nyquist plots). The impedance increases from 3.80 log (Z/ohm) to 3.85 log (Z/ohm) and 3.95 log (Z/ohm), as shown in (Figure 6(b)). (Bode plots). The Bode-phase is shown between 82° and 83°. Hence corrosion is inhibited (Figure 6(c)).

Table 2. The fitted results of EIS using an equivalent circuit for the sample Ni-Ti alloy

Tabela 2. Prilagođeni rezultati EIS-a korišćenjem ekvivalentnog kola za uzorak Ni-Ti legure

Days	Alloy	System	Nyquist plot		Bode plot	
			$R_{ct}(\Omega \cdot \text{cm}^2)$	$C_{dl}(\text{F}/\text{cm}^2)$	Impedance $\log(Z/\text{ohm})$	Phase angle (degrees)
1 Day	Ni-Ti	ABP	90	1.766×10^{-8}	3.80	84
		ABP/TFG 0.1 ppm	180	8.83×10^{-9}	3.85	82
		ABP /TFG 0.5 ppm	200	7.8×10^{-9}	3.95	83
10 Days		ABP	80	1.988×10^{-8}	3.90	85
		ABP /TFG 0.1 ppm	190	8.37×10^{-9}	4.15	80
		ABP /TFG 0.5 ppm	340	4.68×10^{-9}	4.35	65
20 Days		ABP	180	8.83×10^{-9}	3.95	81
		ABP /TFG 0.1 ppm	360	4.42×10^{-9}	4.0	84
		ABP /TFG 0.5 ppm	380	4.18×10^{-9}	4.05	86
30 Days	ABP	150	1.06×10^{-8}	3.95	80	
	ABP /TFG 0.1 ppm	180	8.83×10^{-9}	4.20	76	
	ABP /TFG 0.5 ppm	450	3.533×10^{-9}	4.40	84	

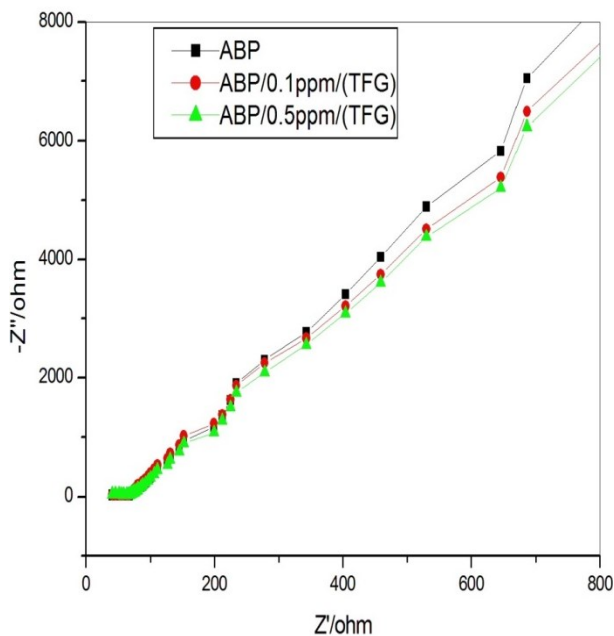


Figure 6(a). Nyquist plots of Ni-Ti alloy in ABP in the absence and presence of 0.1 ppm and 0.5 ppm of TFG seeds for 1 day

Slika 6(a). Najkvistovski dijagrami legure Ni-Ti u ABP u odsustvu i prisustvu 0,1 ppm i 0,5 ppm semena TFG tokom 1 dana

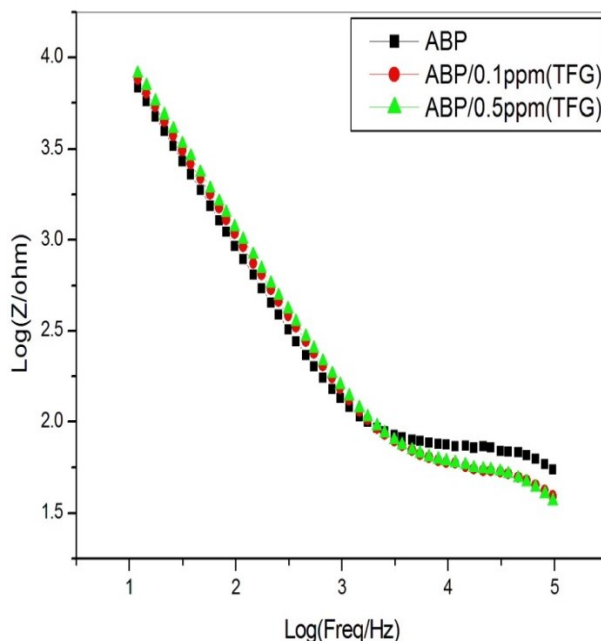


Figure 6(b). Bode plots of Ni-Ti alloy in ABP in the absence and presence of 0.1 ppm and 0.5 ppm of TFG seeds for 1 day

Slika 6(b). Bodeovski dijagrami legure Ni-Ti u ABP u odsustvu i prisustvu 0,1 ppm i 0,5 ppm semena TFG tokom 1 dana

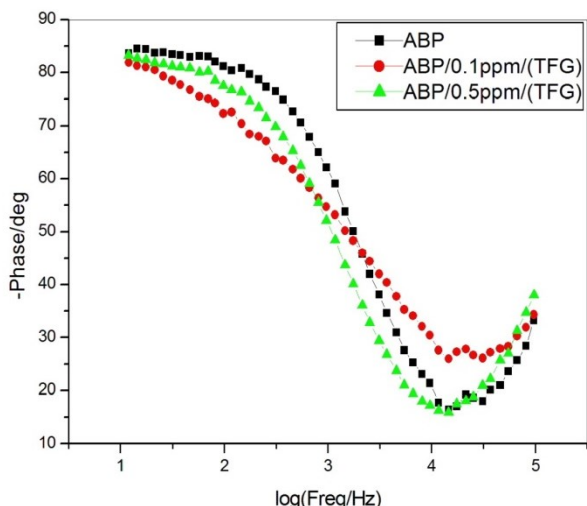


Figure 6(c). Bode plots of Ni-Ti alloy in ABP in the absence and presence of 0.1 ppm and 0.5 ppm of TFG seeds for 1 day

Slika 6(c). Bodeovi grafikoni legure Ni-Ti u ABP u odsustvu i prisustvu 0,1 ppm i 0,5 ppm semena TFG tokom 1 dana

The Ni-Ti alloy is immersed in ABP without TFG seeds for 10 days, the charge transfer resistance (R_{ct}) is 80 ohm.cm². Therefore, the double layer capacitance (C_{dl}) is 1.988×10^{-8} F/cm² shown in (Table 2). The impedance value is 3.90 log (Z/ohm), as shown in (Figure 7(b)). The Bode phase graph shows the phase angle at 85°. Hence, the corrosion process is inhibited. When the Ni-Ti alloy is immersed in ABP containing 0.1 ppm and 0.5 ppm of TFG seeds for 10 days, the R_{ct} value increases from 80 ohm.cm² to 190 ohm.cm² and 340 ohm.cm².

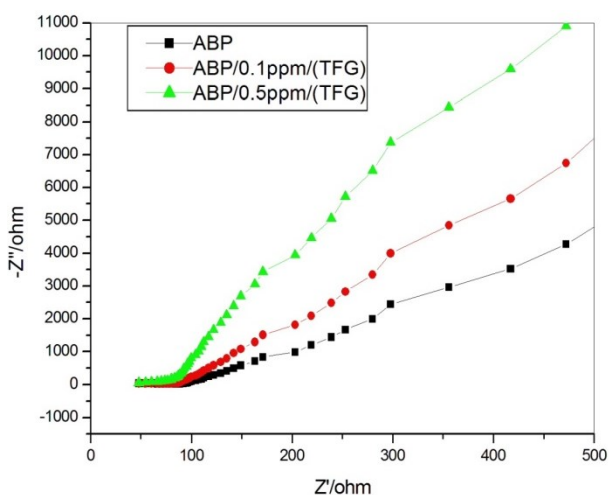


Figure 7(a). Nyquist plots of Ni-Ti alloy in ABP in the absence and presence of 0.1 ppm and 0.5 ppm of TFG seeds for 10 days

Slika 7 (a). Najkvistoviji dijagrami legure Ni-Ti u ABP u odsustvu i prisustvu 0,1 ppm i 0,5 ppm semena TFG tokom 10 dana

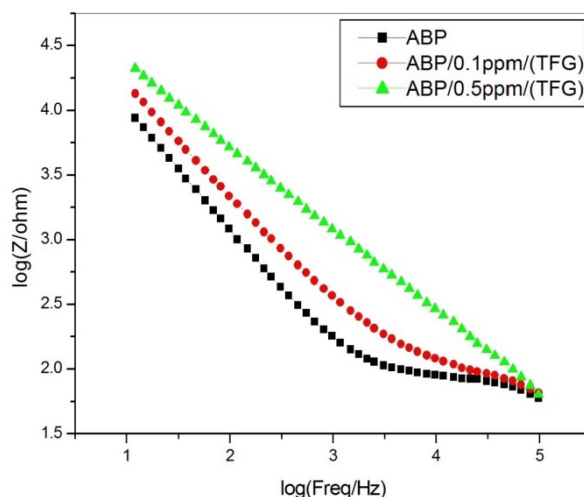


Figure 7(b). Bode plots of Ni-Ti alloy in ABP in the absence and presence of 0.1 ppm and 0.5 ppm of TFG seeds for 10 days

Slika 7(b). Bodeove grafike legure Ni-Ti u ABP u odsustvu i prisustvu 0,1 ppm i 0,5 ppm semena TFG tokom 10 dana

The C_{dl} value decreases from 1.988×10^{-8} F/cm² to 8.37×10^{-9} F/cm² and 4.68×10^{-9} F/cm² shown in (Table 2). (Nyquist plots). The impedance increases from 3.90 log (Z/ohm) to 4.15 log (Z/ohm) and 4.35 log (Z/ohm), as shown in (Figure (b)). (Bode plots). The Bode-phase is shown between 80° and 65°. Hence corrosion is inhibited (Figure 7(c)).

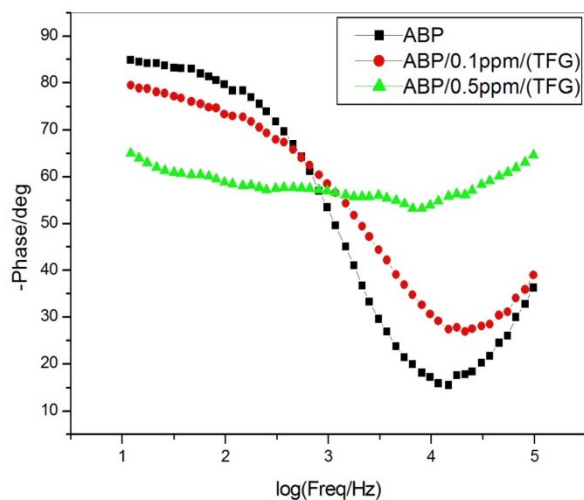


Figure 7(c). Bode plots of Ni-Ti alloy in ABP in the absence and presence of 0.1 ppm and 0.5 ppm of TFG seeds for 10 days

Slika 7(c). Bodeovi grafikoni legure Ni-Ti u ABP u odsustvu i prisustvu 0,1 ppm i 0,5 ppm semena TFG tokom 10 dana

The Ni-Ti alloy is immersed in ABP without TFG seeds for 20 days, the charge transfer resistance (R_{ct}) is 180 ohm.cm². The double layer capacitance (C_{dl}) is 8.83×10^{-9} F/cm², shown in

(Table 2). The impedance value is $3.95 \log(Z/\text{ohm})$, as shown in (Figure 8(b)). The Bode phase graph shows the phase angle at 81° . Hence, the corrosion process is inhibited. When Ni-Ti alloy is immersed in ABP containing 0.1 ppm and 0.5 ppm of TFG seeds for 20 days, the R_{ct} value increases from 180 ohm.cm^2 to 360 ohm.cm^2 and 380 ohm.cm^2 . The C_{dl} value decreases from $8.83 \times 10^{-9} \text{ F/cm}^2$ to $4.42 \times 10^{-9} \text{ F/cm}^2$ and $4.18 \times 10^{-9} \text{ F/cm}^2$, as shown in (Table 2). (Nyquist plots). The impedance value increases from $3.95 \log(Z/\text{ohm})$ to $4.0 \log(Z/\text{ohm})$ and $4.05 \log(Z/\text{ohm})$ shown in (Figure 8(b)). (Bode plots). The Bode-phase has shown the phase angle between 84° and 86° . Hence corrosion is inhibited (Figure 8(c)).

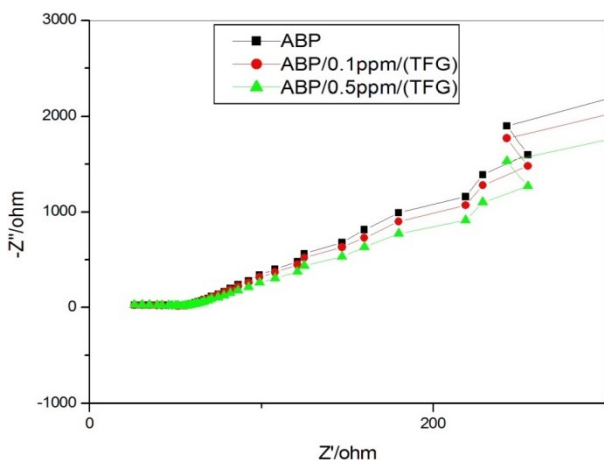


Figure 8(a). Nyquist plots of Ni-Ti alloy in ABP in the absence and presence of 0.1 ppm and 0.5 ppm of TFG seeds for 20 days

Slika 8 (a). Najkvistoviji dijagrami legure Ni-Ti u ABP u odsustvu i prisustvu 0,1 ppm i 0,5 ppm semena TFG tokom 20 dana

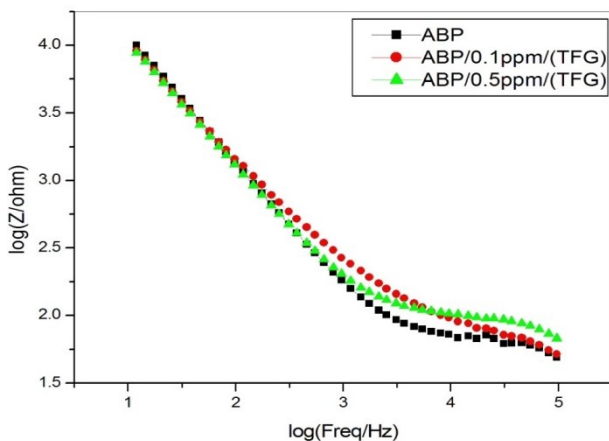


Figure 8(b). Bode plots of Ni-Ti alloy in ABP in the absence and presence of 0.1 ppm and 0.5 ppm of TFG seeds for 20 days

Slika 8(b). Bodeove grafike legure Ni-Ti u ABP u odsustvu i prisustvu 0,1 ppm i 0,5 ppm semena TFG tokom 20 dana

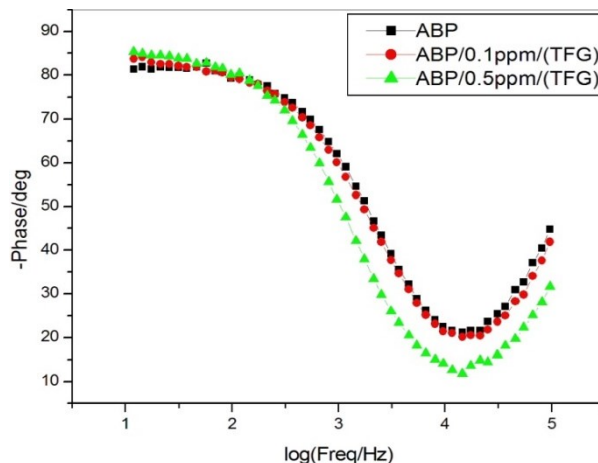


Figure 8(c). Bode plots of Ni-Ti alloy in ABP in the absence and presence of 0.1 ppm and 0.5 ppm of TFG seeds for 20 days

Slika 8(c). Bodeovi grafikoni legure Ni-Ti u ABP u odsustvu i prisustvu 0,1 ppm i 0,5 ppm semena TFG tokom 20 dana

The Ni-Ti alloy is immersed in ABP without TFG seeds for 30 days, the charge transfer resistance (R_{ct}) is 150 ohm.cm^2 . The double layer capacitance (C_{dl}) is $1.06 \times 10^{-8} \text{ F/cm}^2$, shown in (Table 2). The impedance value is $3.95 \log(Z/\text{ohm})$, as shown in (Figure 9(b)). The Bode phase graph shows the phase angle is 80° . So the corrosion process is inhibited. When Ni-Ti alloy is immersed in ABP containing 0.1 ppm and 0.5 ppm of TFG seeds for 30 days, the R_{ct} value increases from 150 ohm.cm^2 to 180 ohm.cm^2 and 450 ohm.cm^2 .

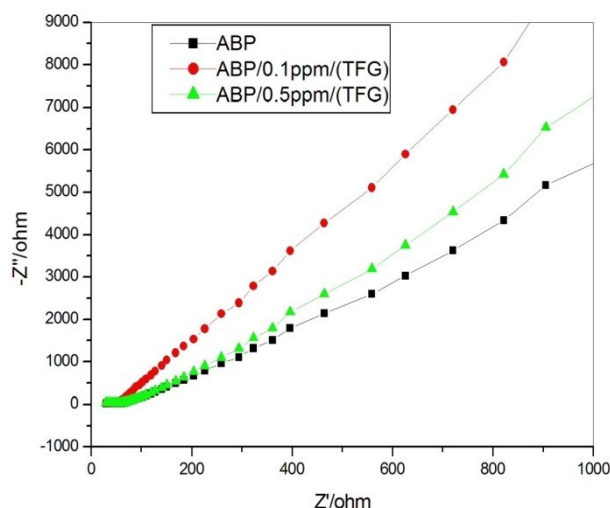


Figure 9(a). Nyquist plots of Ni-Ti alloy in ABP in the absence and presence of 0.1 ppm and 0.5 ppm of TFG seeds for 30 days

Slika 9(a). Najkvistoviji dijagrami legure Ni-Ti u ABP u odsustvu i prisustvu 0,1 ppm i 0,5 ppm semena TFG tokom 30 dana

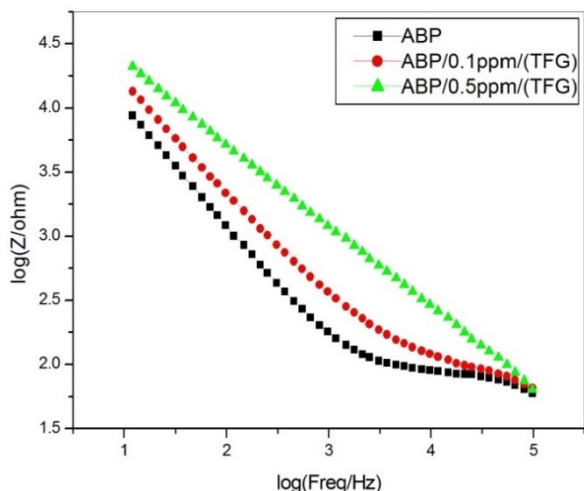


Figure 9(b). Bode plots of Ni-Ti alloy in ABP in the absence and presence of 0.1ppm and 0.5 ppm of TFG seeds for 30 days

Slika 9(b). Bodeove grafike legure Ni-Ti u ABP u odsustvu i prisustvu 0,1 ppm i 0,5 ppm semena TFG tokom 30 dana

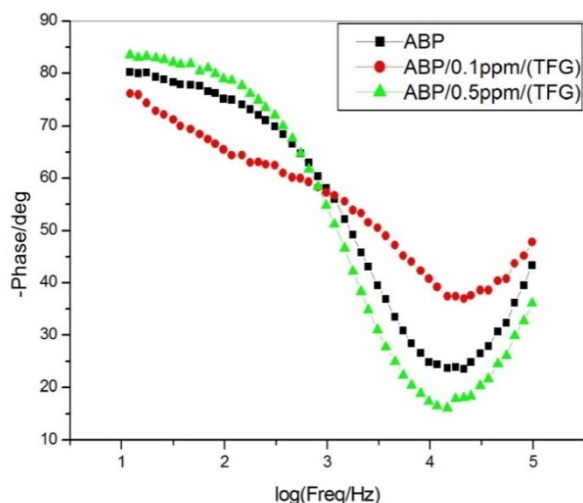


Figure 9(c). Bode plots of Ni-Ti alloy in ABP in the absence and presence of 0.1ppm and 0.5 ppm of TFG seeds for 30 days

Slika 9(c). Bodeovi grafikoni legure Ni-Ti u ABP u odsustvu i prisustvu 0,1 ppm i 0,5 ppm semena TFG tokom 30 dana

The C_{dl} value decreases from 1.06×10^{-8} F/cm² to 8.83×10^{-9} F/cm² and 3.533×10^{-9} F/cm², as shown in Table 2. (Nyquist plots). The impedance value increases from 3.95 log (Z/ohm) to 4.20 log (Z/ohm) and 4.40 log (Z/ohm), as shown in (Figure 9(b)). (Bode plots). The Bode-phase is shown between 76° and 84°. Hence, the corrosion is inhibited (Figure 9(c)).

From the results, the charge transfer resistant value (R_{ct}) and impedance value increase while the double-layer capacitance value decreases because

double-layer capacitance is inversely related to charge transfer resistance [19].

The semi-circle diameter was significantly smaller in the absence of TFG seeds than in the presence of 0.1 ppm and 0.5 ppm of TFG seeds, as shown in Figure 6(a-d). The largest semi-circle diameter indicates the lowest corrosion rate, according to a comparison of the Nyquist diagrams for the three scenarios.

It is fascinating to note that the Ni-Ti alloys in the presence of TFG seeds at 0.1 ppm and 0.5 ppm concentrations are immersed for 1, 10, 20, and 30 days, the rate of corrosion decreases and the C_{dl} decreases, thereby showing in the R_{ct} increase. This indicates that a compelling protective film was formed more on the Ni-Ti alloy surface in the presence of TFG seeds for 30 days.

3.4. Scanning Electron Microscope

SEM micrographs of the surface are examined to understand the nature of the surface film in the absence and presence of inhibitors and the extent of the corrosion of Ni-Ti alloy [22, 23]. The SEM images of different magnifications (X500, X3.50K, and X2.00K) of Ni-Ti alloy specimens immersed in ABP in the absence and presence of additive systems are shown in Figure 10 a, b and c respectively.

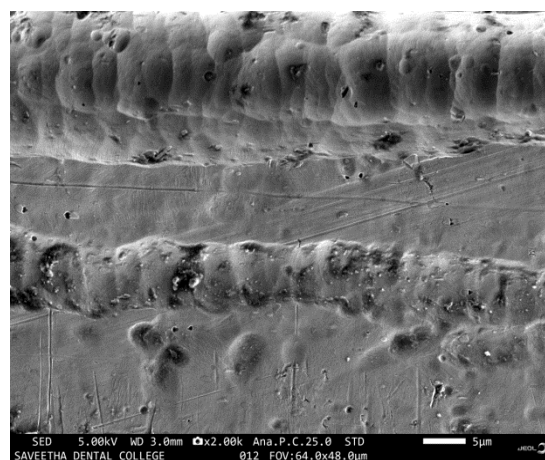


Figure 10 (a). SEM image of blank Ni-Ti alloy

Slika 10 (a). SEM slika polirane prazne legure Ni-Ti

The SEM proposes an illustrative demonstration of the Ni-Ti alloy surface. The SEM micrographs of the surface are examined. The SEM metaphors of blank Ni-Ti alloy are shown in Figure 10 (a) on the smooth surface of the alloy. This indicates the absence of corrosion products on the metal surface. The SEM metaphors of Ni-Ti alloy exposed in ABP have shown in Figure 10(b), designate the minor roughness of the alloy surface, which indicates the corrosion of Ni-Ti alloy in ABP (Figure 10(c)) shows that the presence of 0.5 ppm of TFG seeds in ABP at 30 days.

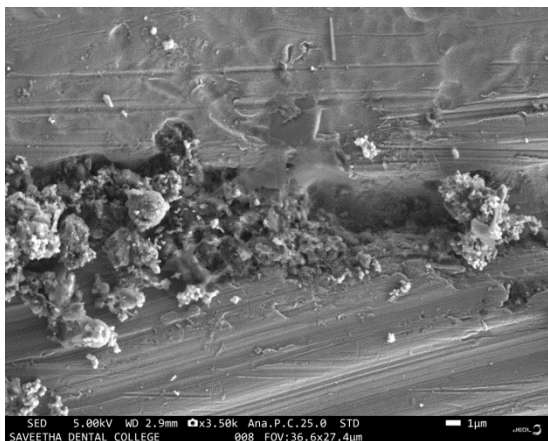


Figure 10 (b). SEM image of Ni-Ti alloy / ABP

Slika 10 (b). SEM slika legure Ni-Ti / ABP

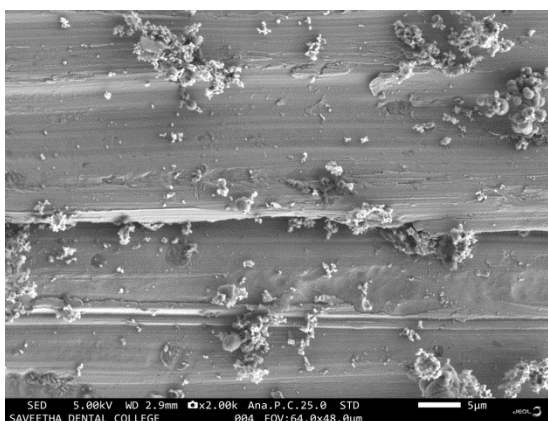


Figure 10 (c). SEM image of Ni-Ti alloy / ABP / TFG seeds

Slika 10 (c). SEM slika legure Ni-Ti / ABP / TFG semena

The surface coverage improvement is due to the formation of insoluble complexes on the alloy surface, which efficiently controls the dissolution of the Ni-Ti alloy.

3.5. Energy Dispersive Analysis of X-rays

The EDAX spectra were used to determine the elements present on the alloy surface before and after exposure to the inhibitor solution. The objective of this section was to confirm the results obtained from electrochemical measurements that a protective surface film of inhibitor is formed on the alloy surface. To achieve this, EDAX examinations of the alloy surface were performed in both the absence and presence of additive systems [24-27].

The EDAX spectrum of blank Ni-Ti alloy has shown in Figure 11(a). The chemical compositions have shown Ni = 50.1, Ti = 40.2, and C = 9.7, respectively. The Ni-Ti alloy immersed in ABP containing 0.5 ppm of TFG seeds has shown in Figure 11(c). It shows the additional line characteristics for Na = 2.5, Ca = 7.8, P = 4.0, and Cl = 1.4. In addition, the intensity of the N = 25.2 signal is enhanced. The appearance of the Na and Ni signals and this enhancement in N and S are due to inhibitors (TFG seeds). These data show that the alloy surface is covered by P, N, Na, Cl, and Ca atoms have shown in Figure 11(c) demonstrates that, compared to those seen in ABP Figure 11(b), the Ni peaks seen in the presence of inhibitors are significantly decreased. The suppression of the Ni peaks occurs because of the overlying inhibitor film. This observation indicates the existence of an adsorbed layer of inhibitor that protects Ni-Ti alloy against corrosion. These results suggest that the N, P, Cl, Ca, and S atoms of TFG seeds have coordinated with Ni-Ti alloy complex. The anodic sites of the Ni-Ti alloy surface exhibit TFG seed complexes, while the cathodic sites of the alloy surface exhibit Ca atom precipitation in the form of superhydrophobic coatings.

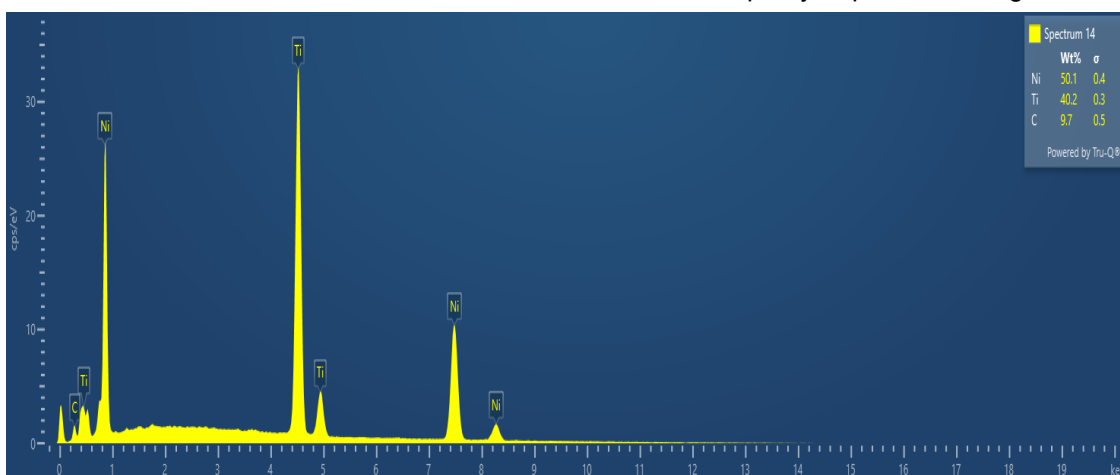


Figure 11 (a). EDAX of polished Ni-Ti alloy

Slika 11 (a.) EDAX od polirane legure Ni-Ti

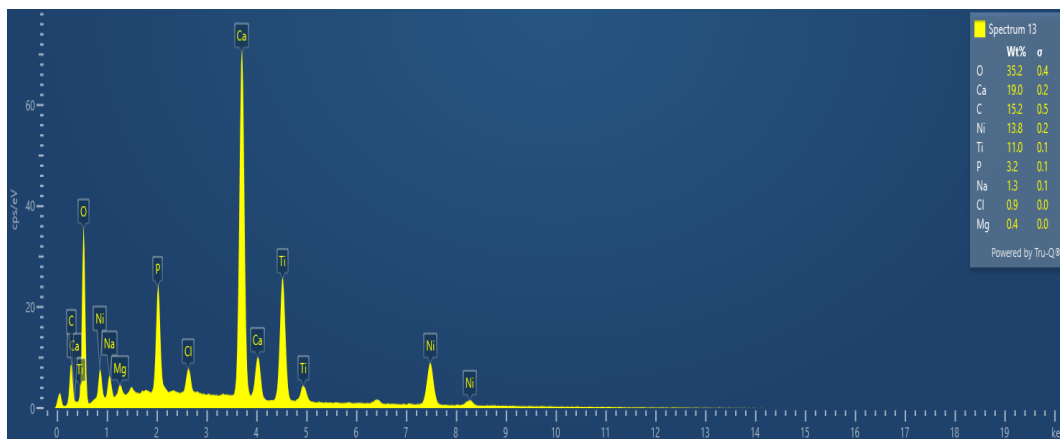


Figure 11 (b). EDAX of polished Ni-Ti alloy / ABP

Slika 11 (b). EDAKS od polirane legure Ni-Ti / ABP

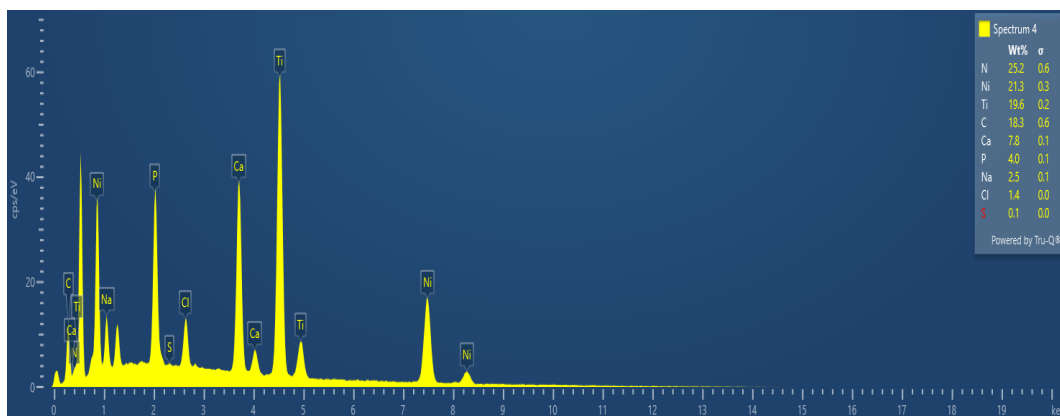


Figure 11 (c). EDAX of polished Ni-Ti alloy / ABP / TFG seeds

Slika 11 (c). EDAKS od polirane legure Ni-Ti / ABP / TFG semena

3.6. Atomic Force Microscope

Atomic force microscopy is a practical method for obtaining surface roughness data. AFM is becoming an accepted method of roughness investigation [26, 28].

The atomic force microscopy images were obtained with the help of AFM-Ntegra Prima, NTMDT, and Ireland incorporation. AFM instrument operating in contact mode in the air. The scan size of all the AFM images is 10 μm x 10 μm areas at a scan rate of 1 line/sec, and the scanning direction is horizontal. The varying scan rate depends upon

the frequency and scanning area of the sample. AFM study is created for the best system of Ni-Ti alloy in TFG used as an inhibitor.

The analysis of an atomic force microscope (AFM) is a suitable method for collecting roughness indicators from various surfaces. The three-dimensional (3D) morphologies are present in the polished Ni-Ti alloy surface, the Ni-Ti alloy treated to artificial blood plasma, and 0.5 ppm of TFG at 30 days.

Table 3. AFM Analysis for Ni-Ti alloy exposed in the presence and absence of TFG seeds

Tabela 3. AFM analiza za Ni-Ti leguru izloženu u prisustvu i odsustvu TFG semena

Samples	RMS, (Sq) Roughness (nm)	Average, (Sa) Roughness (nm)	Maximum Peak-to-peak valley Height, (nm)	Coefficient of Kurtosis (S _{ka})	Entropy	Surface Skewness (S _{sk})
Refined, Ni-Ti	20.95	15.30	430.64	6.74	9.55	0.088
ABP /Ni-Ti	46.16	28.16	648.3	18.26	10.34	2.94
ABP/Ni-Ti /TFG 0.5 ppm	54.26	39.87	860.86	9.48	10.11	1.30

AFM analysis was performed to attain the Average roughness (Sa), Root-mean-square roughness (Sq), and the maximum peak-to-peak valley (P-v) height values. These values for Ni-Ti alloy exposed in the different environments are summarized in Table 3.

Figure 12 (a) shows the surface topography of the polished Ni-Ti alloy surface. The Sa, Sq, and P-v height data for the refined Ni-Ti alloys are 15.30 nm, 20.95 nm, and 430.64 nm, correspondingly. These data designate the surface of Ni-Ti alloy as identical. The slight roughness discovered in the refined Ni-Ti alloy is due to atmospheric corrosion Figure 12(b) shows the pitting corrosion Ni-Ti alloy without Trigonella

foenum-graecum engaged in ABP of Sa, Sq, and P-v data get for the refined Ni-Ti alloys is 28.16 nm, 46.16 nm, and 648.3 nm, correspondingly. These data designate the surface of Ni-Ti alloy with superior roughness to the refined Ni-Ti alloy. The Figure 12(c) shows the Ni-Ti alloy in ABP comprising 0.5 ppm of Trigonella foenum-graecum seeds. The data of Sa, Sq, and P-v height values for the refined Ni-Ti alloys are 39.87 nm, 54.26 nm, and 860.86 nm, correspondingly. These data designate that the surface of Ni-Ti alloy values is prominently high. These data also designate the surface of Ni-Ti alloy as superior roughness to the refined Ni-Ti alloy. These aspects authorize that the surface is smooth, and a strong shielding layer bounds the surface of the metal layer.

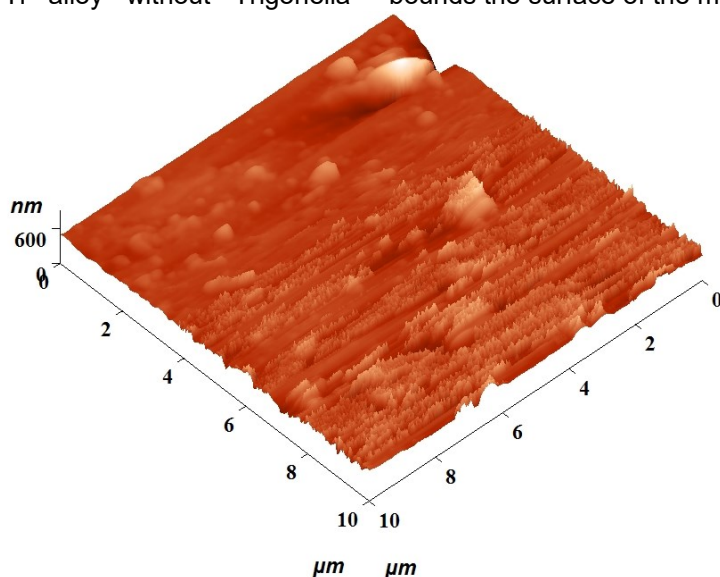


Figure 12 (a). AFM image of Ni-Ti alloy

Slika 12 (a). AFM slika legure Ni-Ti

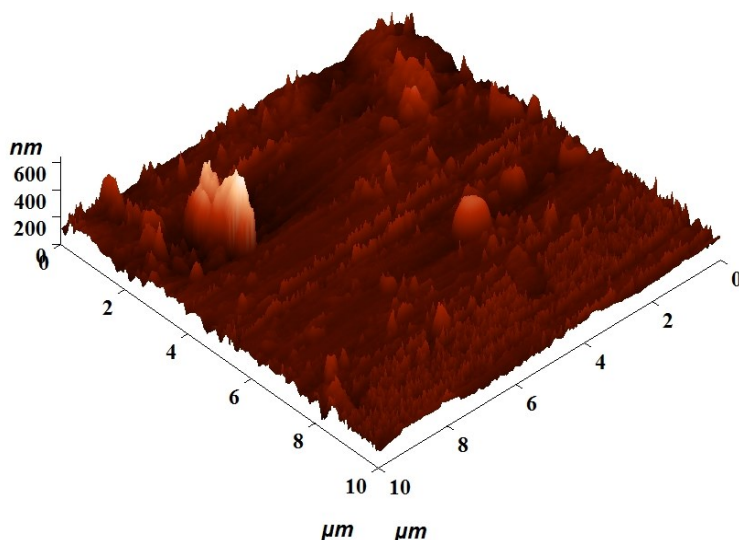


Figure 12 (b). AFM image of Ni-Ti alloy / ABP

Slika 12 (b). AFM slika legure Ni-Ti / ABP

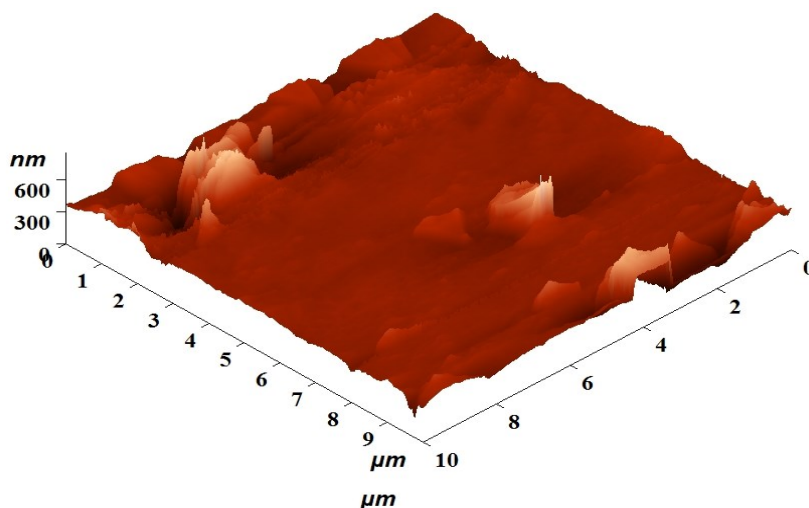


Figure 12 (c). AFM image of Ni-Ti alloy / ABP / TFG seeds

Slika 12 (c). AFM slika legure Ni-Ti / ABP / TFG semena

The entropy values for polished Ni-Ti alloy in ABP and Ni-Ti alloy in artificial blood plasma comprising 0.5 ppm of TFG seeds decline progressively. It demonstrates that the Ni-Ti alloy corrosion resistance increases. Surface skewness (S_{sk}) is a statistical parameter to explain the amplitude distribution function, which indicates the probability that a profile of the surface has a certain height at any position. A surface with low skewness shows a porous surface with fairly deep valleys in a smoother plateau for refined Ni-Ti alloy. The Ni-Ti alloy exposed in ABP surfaces with high skewness shows the raised surface has relatively high spikes that bulge above a flatter average for Ni-Ti alloy exposed with TFG seeds engaged in ABP. Kurtosis is associated with the spikiness of the profile. The polished Ni-Ti alloy, Ni-Ti alloy in ABP, and Ni-Ti

alloy in ABP comprising 0.5 ppm of TFG seeds, Kurtosis distribution, has few high peaks and low value comparatively flat surface. It is decided that the Ni-Ti alloy in ABP comprising 0.5 ppm of TFG seeds is more corrosion resistant than the polished Ni-Ti alloy and Ni-Ti alloy in ABP.

3.7. X-ray diffraction analysis

XRD patterns of the Ni-Ti alloy and Ni-Ti alloy in ABP in the presence of TFG seeds have shown in Figure 13(a) and Figure 13(b). It can be seen from XRD patterns that blank Ni-Ti alloy shows two prominent diffraction peaks between 20 and 80. The prominent peaks at 42.3 (110) and 77.5 (211) belong to the Ni-Ti phase [29].

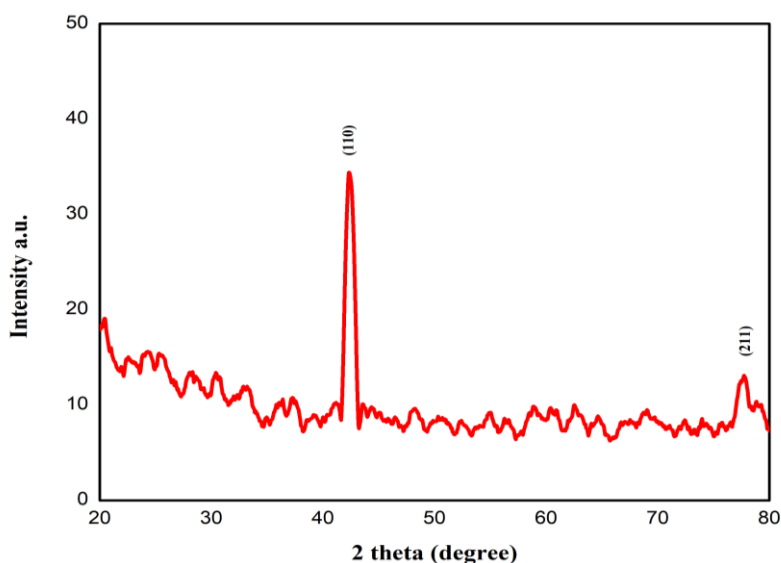


Figure 13 (a). XRD pattern of Ni-Ti alloy

Slika 13 (a). XSRD uzorak legure Ni-Ti

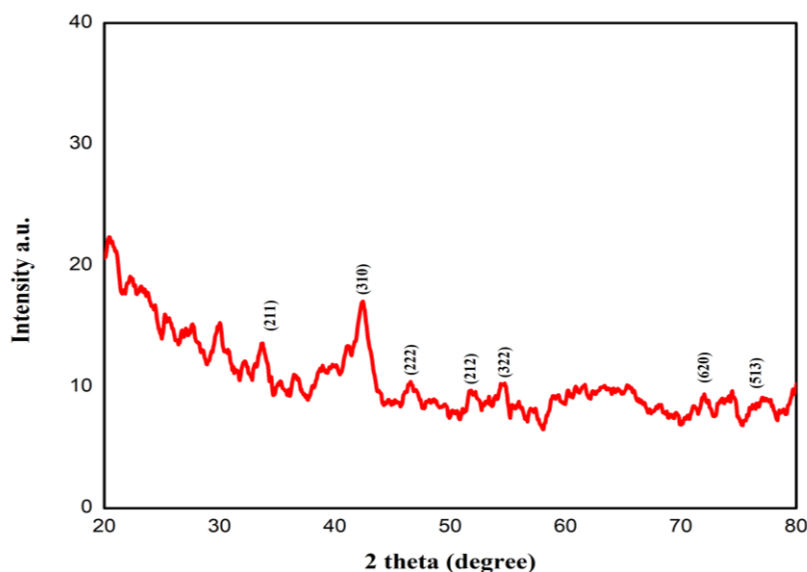


Figure 13 (b). XRD pattern of Ni-Ti alloy / ABP / TFG seeds

Slika 13 (b). KSRD uzorak legure Ni-Ti / ABP / TFG semena

After being immersed in TFG seeds implantation and anodization, a stable characteristic peak of rutile TiO_2 appears, as seen in their diffraction patterns in Figure 13(b). These results show the formation of a TiO_2 layer on the Ni-Ti Surface [30]. The HA on Ni-Ti alloy in ABP in the presence of TFG seeds was identified using an XRD investigation. As a result, the sample contains HA, as shown by the XRD analysis results in Figure 13(b).

The first three more significant peaks of intensity in the diffraction pattern of HA powder shown by XRD examination, the first three more significant peaks of intensity located between the angular zone $30 < 2\theta < 50$ were assigned corresponded to the Miller indices of 211, 310, and 222. Although such indexes are associated with HA, no isolated peaks with a lower intensity are present, indicating that crystallinity is not very high [31]. However, a comparison between the obtained HA XRD patterns and the JCPDS 09-432 file shows that HA powder obtained by the wet precipitation method represents the typical HA pattern [32].

4. CONCLUSION

It is fascinating to note that the Ni-Ti alloy in the presence of TFG seeds at 0.1 ppm and 0.5 ppm concentrations are immersed for 1, 10, 20 and 30 days, the rate of corrosion decreases, and the corrosion current also decreases, thereby showing in the LPR, I_{corr} , C_{dl} and R_{ct} values. This indicates that a compelling protective film is formed on the alloy surface in the presence of TFG seeds. Thus, the polarisation study and AC impedance spectral

study leads to the conclusion that the corrosion resistance of Ni-Ti alloys in ABP in the presence of TFG seeds of 0.1 ppm and 0.5 ppm for 1, 10, 20, and 30 days is in the following order:

$$30 \text{ days} > 20 \text{ days} > 10 \text{ days} > 1 \text{ day}$$

According to the description above, the 30 days of immersion operate as a more corrosion-resistant phase than other times because LPR increases while I_{corr} decreases, the rate of corrosion decreases and the C_{dl} decreases, thereby showing in the R_{ct} increase. This indicates that a compelling protective film was formed on the Ni-Ti alloy surface in the presence of TFG seeds.

The SEM has validated the superhydrophobic coatings surface morphology. EDAX has determined the elemental compositions of Ni-Ti alloys and ABP in the presence of TFG seeds. Using AFM and XRD, the topography and apatite formation complexes of the Ni-Ti alloy are investigated.

The electrochemical behaviour of Ni-Ti alloys in ABP was studied for 1, 10, 20, and 30 days, with and without TFG seeds. As a result of the discussions above, the anticorrosive coating layer of the alloy is formed for an increasing number of days. In addition, the alloys hydroxyapatite layer is formed for an increased number of immersion days. As a result of the preceding discussions, we conclude that ingesting any of the *Trigonella foenum-graecum* for a person with Ni-Ti alloy implanted will strengthen their immune system and create an anticorrosive layer. These Ni-Ti alloys underwent the observed electrochemical modifications.

5. REFERENCES

- [1] M.A.Siyah, R.Moradian, I.Manouchehri (2019) Electrochemical impedance spectroscopy (EIS) study of modified SS316L using radio frequency sputtering Ti6Al4V coating in ringer solution, *Anti-Corrosion Methods and Materials.*, 66(1), 27-33. <https://doi.org/10.1108/ACMM-05-2018-1929>.
- [2] M.Gojic, L.Vrsalovic, S.Kozuh, D.Cubela, S. Gudic (2012) Microstructure and corrosion properties Ni-Ti alloy after electrochemical testing in 0.9% NaCl solution, *Zaštita materijala.*, 53(4), 345-351. (http://idk.org.rs/wp-content/uploads/2013/12/ZM_53_4_345.pdf.)
- [3] S.A.Fadlallah, N.El-Bagoury, S.M.G.El-Rab, R.A.Ahmed, G.El-Ousamii (2014) An overview of Ni-Ti shape memory alloy: Corrosion resistance and antibacterial inhibition for dental application, *J. of Alloys and Compounds.*, 583, 455-464. <https://doi.org/10.1016/j.jallcom.2013.08.029>.
- [4] S.A.Shabalovskaya, G.C.Rondelli, A.L.Undisz, J.W. Anderegg, T.D.Burleigh, M.E.Rettenmayr (2009) The electrochemical characteristics of native Nitinol surfaces, *Biomaterials.*, 30(22), 3662-3671. <https://doi.org/10.1016/j.biomaterials.2009.03.034>.
- [5] F.Stergioudi, C.A.Vogiatzis, E.Pavlidou, S. Skolianos, N.Michailidis (2016) The corrosion resistance of porous NiTi biomedical alloy in simulated body fluids, *Innovative Materials and Structures.*, 25(9), 095024. <http://dx.doi.org/10.1088/0964-1726/25/9/095024>.
- [6] T.Hu, C.Chu, Y.Xin, S.Wu, K.W.Yeung, P.K.Chu (2010) Corrosion products and mechanism on NiTi shape memory alloy in a physiological environment, *Journal of Materials Research.*, 25(2), 350-358. <https://doi.org/10.1557/JMR.2010.0051>.
- [7] T.Hu, Y.C. Xin, S.L.Wu, C.L.Chu, J.Lu, L.Guan, P.K.Chu (2011) Corrosion behaviour on orthopedic Ni-Ti alloy with nanocrystalline/amorphous surface, *Materials Chemistry and Physics.*, 126(1-2), 102-107. <https://doi.org/10.1016/j.matchemphys.2010.11.061>.
- [8] S.Acharya, A.Srichamroen, S.Basu, B. Ooraikul, T.Basu (2006) Improvement in the nutraceutical properties of fenugreek (*Trigonella foenum-graecum* L.), *Songklanakarin J. Sci. Technol.*, 28(1), 1-9. (<https://www.thaiscience.info/journals/Article/SONG/10462627.pdf>.)
- [9] M.Aasim, F.S.Baloch, A.Bakhsh, M. Sameeullah, K.M.Khawar (2018) Biotechnological approaches for genetic improvement of fenugreek (*Trigonella foenum-graecum* L.) Biotechnological Approaches for Medicinal and Aromatic Plants Conservation, *Genetic Improvement and Utilization.*, p.417-444. https://doi.org/10.1007/978-981-13-0535-1_19.
- [10] D.Tiran, (2003) The use of fenugreek for breastfeeding women. *Complementary Therapies in Nursing and Midwifery.*, 3(9), 155-156. [http://dx.doi.org/10.1016%2F%2FS1353-6117\(03\)00044-1](http://dx.doi.org/10.1016%2F%2FS1353-6117(03)00044-1).
- [11] E.K.Kalra (2003) Nutraceutical definition and introduction, *Aaps Pharmsci.*, 5(3), 27-28. <https://doi.org/10.1208/ps050325>.
- [12] W.Kajzer, A.Krauze, W.Walke, J.Marciniak (2008) Corrosion behavior of AISI 316L steel in artificial body fluids, *Journal of Achievements in Materials and manufacturing engineering.*, 31(2), 247-253. (https://www.researchgate.net/profile/AnitaKajzer/publication/268808675_Kajzer_Krauze_Walke_Marciniak_Journal_of_Achievements_in_Materials_and_Manufacturing_Engineering/links/54772a190cf2a961e48240bd/Kajzer-Krauze-Walke-Marciniak-Journal-of-Achievements-in-Materials-and-Manufacturing-Engineering.pdf, 01.12.2008.)
- [13] G.A.Petropoulos (2002) Fenugreek: the genus *Trigonella.*, CRC Press. <https://doi.org/10.4324/9780203217474>.
- [14] F.R.García-Galvan, S.Fajardo, V.Barranco, S.Feliu (2021) Experimental apparent stern–geary coefficients for AZ31B Mg alloy in physiological body fluids for accurate corrosion rate determination, *Metals.*, 11(3), 391. <https://doi.org/10.3390/met11030391>.
- [15] A.C.C.Mary, S.Rajendran, H.Al-Hashem, R.J. Rathish, T.Umasankareswari, J.Jeyasundari (2015) Corrosion resistance of mild steel in simulated produced water in presence of sodium potassium tartrate, *Int. J. Nano Corr. Sci. Eng.*, 1, 42-50. (https://www.researchgate.net/profile/Susai-Rajendran/publication/272834126_Corrosion_Resistance_Of_Mild_Steel_In_Simulated_Produced_Water_In_Presence_Of_Sodium_Potassium_Tartrate/links/54f1c2650cf2f9e34eff053d/Corrosion-Resistance-Of-Mild-Steel-In-Simulated-Produced-Water-In-Presence-Of-Sodium-Potassium-Tartrate.pdf.)
- [16] V.Singh, A.N.Garg (2006) Availability of essential trace elements in Indian cereals, vegetables, and spices using INAA and the contribution of spices to daily dietary intake, *Food Chemistry.*, 94(1), 81–89. doi:10.1016/j.foodchem.2004.10.053 .
- [17] K.Srinivasan (2006) Fenugreek (*Trigonella foenum-graecum*) A review of health beneficial physiological effects, *Food reviews international.*, 22(2), 203–224. <https://doi.org/10.1080/87559120600586315>.
- [18] P.Ojha, P.Prajapati, T.B.Karki (2018) Soaking and germination effect on bioactive components of fenugreek seeds (*Trigonella foenum graecum* L.), *International Food Research Journal.*, 25(2), 690-694. <http://www.ifrj.upm.edu.my/>.
- [19] S.John Mary, G.Puthlibai, P.Kathiravan, J.Mano Deepa, A.Selvam (2021) Electrochemical behavior of Ni-Ti (Super-elastic) alloy in the artificial saliva in the presence of Phexin, *Materials Today Proceedings.*, pp. 36, 878–882. <https://doi.org/10.1016/j.matpr.2020.07.022>.
- [20] E.Castaneda, J.G.Gonzalez-Rodriguez, J.Colin, M.A.Neri-Flores (2010) Electrochemical behavior of Ni-Al-Fe alloys in simulated human body solution, *Journal of Solid State Electrochemistry.*, 14, 1145-1152. <https://doi.org/10.1007/s10008-009-0941-z>
- [21] S.John Mary, S.Rajendran (2013) Corrosion Behaviour of SS316L in Artificial Blood Plasma in the Presence of Amoxicillin, *Portugaliae Electrochimica Acta.*, 31(1), 33-40. doi: 10.4152/pea.201301033.
- [22] S.R.Paital, N.B.Dahotre (2009) Calcium phosphate coatings for bio-implant applications Materials performance factors and methodologies, *Materials Science and Engineering: R: Reports.*, 66(1-3), 1-70. <https://doi.org/10.1016/j.mser.2009.05.001>.

- [23] V.A.Brigitta, C.Thangavelu, S.Rajendran (2019) Effects of tablet on orthodontic wire made of SS 316L alloy in Artificial Saliva, International J. of Research and Analytical Reviews., 6,1000-1005. (https://www.researchgate.net/profile/SusaiRajendran/publication/332303320_Effects_of_Tablet_on_Orthodontic_Wire_made_of_SS316L_Alloy_in_Artificial_Saliva/links/5cacadf00458515cd2b0d266c/Effects-of-Tablet-on-Orthodontic-Wire-made-of-SS316L-Alloy-in-Artificial-Saliva.pdf.)
- [24] A.Abdal-Hay, H.A.Fouad, B.Alshammari, K.A. Khalil (2020) Biosynthesis of bonelike apatite 2D nanoplate structures using fenugreek seed extract, Nanomaterials., 10(5), 919. <https://doi.org/10.3390/nano10050919>.
- [25] M.A.Hussein, M.Kumar, R.Drew, N.Al-Aqeeli (2017) Electrochemical corrosion and in vitro bioactivity of nano-grained biomedical Ti-20Nb-13Zr alloy in a simulated body fluid, Materials., 11(1), 26-35. <http://dx.doi.org/10.3390/ma11010026>.
- [26] R.Nagalakshmi, L.Nagarajan, R.J.Rathish, S.S. Prabha, N.Vijaya, J.Jeyasundari, S.Rajendran (2014) Corrosion resistance of SS316L in artificial urine in presence of D-glucose, Int. J. Nano. Corr. Sci. Engg., 1(1), 39-49. (https://www.researchgate.net/profile/SusaiRajendran/publication/272743214_Corrosion_Resistance_Of_SS316L_In_Artificial_Urine_In_Presence_Of_D-Glucose/links/54ecaa6f0cf27bfd7713d7d/Corrosion-Resistance-Of-SS316L-In-Artificial-Urine-In-Presence-Of-D-Glucose.pdf.)
- [27] Y.C.Hong, D.H.Shin, S.C.Cho, H.S.Uhm (2006) Surface transformation of carbon nanotube powder into super-hydrophobic and measurement of wettability, Chem.Phys.Lett., 427(4-6), 390-393. doi:10.1016/j.cplett.2006.06.033.
- [28] J.C.Souza, S.L.Barbosa, E.A.Ariza, M.Henriques, W.Teughels, P.Ponthiaux, J.P.Celis, L.A. Rocha (2015) How do titanium and Ti6Al4V corrode in the fluoridated medium as found in the oral cavity? An in vitro study, Materials Science and Engineering: C., 47, 384-393. <https://doi.org/10.1016/j.msec.2014.11.055>.
- [29] P.Kowalski, B.Losiewicz, T.Goryczka (2015) Deposition of chitosan layers on Ni-Ti shape memory alloy, "Archives of Metallurgy and Materials", 1, 171-176. <http://dx.doi.org/10.1515/amm-2015-0027>.
- [30] S.Viswanathan, L.Mohan, P.Bera,C.Anandan (2016) Effect of oxygen plasma immersion ion implantation on the formation of nanostructures over Ni-Ti alloy, RSC advances., 6(78), 74493-74499. <https://doi.org/10.1039/C6RA11541A>.
- [31] D.Malina, K.Biernat, A.Sobczak-Kupiec (2013) Studies on the sintering process of synthetic hydroxyapatite, Acta Biochimica Polonica., 60(4), 851-855. <https://pubmed.ncbi.nlm.nih.gov/24432345/>.
- [32] L.D.Guillen-Romero, M.T.Oropeza-Guzman, E.A. Lopez-Maldonado, A.L.Iglesias, J.A.Paz-Gonzalez, T.Ng, E.Serena-Gomez, L.J.Villarreal-Gomez (2019) Synthetic hydroxyapatite and its use in bioactive coatings, Journal of applied biomaterials & functional materials., 17(1), 2280800018817463. <https://doi.org/10.1177/2280800018817463>

IZVOD

ELEKTROHEMIJSKE AKTIVNOSTI NI-TI LEGURE U VEŠTAČKOJ KRVNOJ PLAZMI SA SEMENOM TRIGONELLA *Foenum graecum*

Istraživano je elektrohemijско ponašanje legure Ni-Ti kada je izložena veštačkoj krvnoj plazmi (ABP) u prisustvu 0,1 i 0,5 ppm semena *Trigonella foenum graecum* (TFG) tokom 1, 10, 20 i 30 dana. Studije o impedansi i polarizaciji naizmenične struje su pokazale da se zaštitni premaz formira na površini metala dok sprečava koroziju. Zaštitni film je formiran na površini legure Ni-Ti implantata, povećan je otpor linearne polarizacije (LPR), a vrednost struje korozije (I_{corr}) je smanjena. Vrednost otpornosti na prenos naelektrisanja (R_{ct}) i vrednost impedanse se povećavaju, a vrednost kapacitivnosti dvoslojnog sloja se smanjuje. Morfologija zaštitnih slojeva i elementarni sastav analizirani su pomoću SEM/EDAX. Svoјstvo zaštitnog filma na leguri Ni-Ti ispitano je atomskim mikroskopom. Analiza difrakcije rendgenskih zraka je potvrdila prirodu apatita. Efikasnost inhibicije korozije legure Ni-Ti u ABP u prisustvu TFG semena u različitim koncentracijama za različito vreme je poboljšana i zaštićena.

Ključne reči: Nikl-titanijum, AFM, zaštitni film, Nyquist dijagrami, Bodeovi dijagrami

Naučni rad

Rad primljen: 25.09.2023.

Rad prihvaćen: 25.10.2023.

Rad je dostupan na sajtu: www.idk.org.rs/casopis